EVALUATION OF OLFACTORY SEARCH ALGORITHMS USING DIRECT NUMERICAL SIMULATION OF TURBULENT SCALAR TRANSPORT

C. F. Panagiotou[1], D. Cerizza [1], T. A. Zaki[2] and Y. Hasegawa[1]

[1] **Institute of Industrial Science, The University of Tokyo, Japan**
[2] **Department of Mechanical Engineering, Johns Hopkins University, Baltimore, USA**

kpan84@iis.u-tokyo.ac.jp

ABSTRACT

In order to locate food and mating partners, animals and insects adopt different strategies which help them to effectively track down the source of the desired chemical substance. They utilize combined information about the wind direction and the odor concentration. Under turbulent conditions, the advection dominates the dispersion of the concentration, and the wind direction can be a most reliable parameter used to track the plume. Inspired by animal behavior, numerous algorithms have been proposed for plume tracking in both air and water, mostly for two-dimensional (2D) motions. In this study, we consider a turbulent channel flow in the presence of a point scalar source. We have conducted direct numerical simulations (DNS) in order to perform a systematic assessment of various existing algorithms, and provide a reliable comparison. Particular focus is laid on the effect of the velocity ratio between flow and sensor movement on the estimation performance. In addition, we propose an extension of one of these algorithms in three dimensions, for which a similar analysis is considered.

INTRODUCTION

The olfactory sense plays a crucial role in the survivor of animals. It is extensively used for a variety of activities such as food tracking, predators avoidance and reproduction. Some animals, such as dogs and rats, are known for exhibiting superior sensitivity. As a result, it is common nowadays for humans to use dogs in a number of tasks, such as rescue operations, detecting landmines or pursuing criminals. Concurrently, the rapid progress in robotics and electronics suggests that robots can potentially be used to fulfill these tasks in the future with a number of advantages relative to animals. For example, animals require extensive training which is associated with significant time and financial resources. In addition, they suffer from fatigue and they can not effectively operate under hazardous conditions, such as toxic environments.

Motivated by the effectiveness of animal search strategies, researchers focused on developing odor source localization algorithms that mimic the behavior of the animals and insects. A widely adopted category of algorithms is reactive algorithms. They are called 'reactive' because their actions are reactions directly related to the sensory input taken from the environment: In the presence of wind, advection dominates the slow diffusion rate, carrying the molecules of the substance and spreading them in regions downstream of the source, often yielding elaborate mixing patterns in turbulent flows. These patterns can take the form of isolated packets, that is regions of high concentration surrounded by regions of very low concentration, forming a rather complex landscape. Under these conditions, the direction of the airflow carrying the substance molecules is more reliable directional cue than concentration gradients in finding the substance source, as recommended by Ishida *et al.* (2012). Consequently, many insects, such as moths, evolved the anemotactic strategy, that is the insect simply moves upwind in the presence of an attractive odor, as noted by Kennedy & Marsh (1974). When sensing a chemical patch, moths surge upwind, while during the absence of patch detection, they either perform crosswind motions with gradually increasing widths, a behavior called casting. Another typical searching behavior is a spiraling motion, commonly observed in walking insects, such as ants, as denoted by Muller & Wehner (1994), that is move around circles with progressively increasing radius. In addition, Voges *et al.* (2014) proposed strategies which combine surge upwind and a two-step plume-tracking strategy, consisting of crosswind casting (zigzaging) followed by spiraling movements. Consequently, various reactive strategies have been proposed based on the insects movements.

A well-known advantage of conducting experiments against numerical simulations is that they allow testing of algorithms in a more natural and complex environment. On the other hand, in computations we can control a flow condition and perform systematic evaluation of different algorithms under reproducible conditions. This provides a unique opportunity to understand the characteristics of locating a scalar source in each algorithm by comparing the sensor movement with the surrounding instantaneous flow and concentration fields. Such information should be useful for optimizing various parameteres in existing olfactory searching algorithms, and also developing novel strategies.

NUMERICAL SET UP

We consider a turbulent channel flow with an embedded point source that releases a passive scalar. The friction Reynolds number $Re_\tau = \frac{u_\tau h}{\nu}$ is 150, where ν is the kinematic viscosity, u_τ is the friction velocity and h is the half-

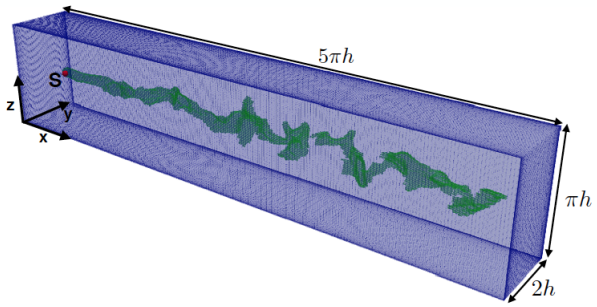

Figure 1: Schematic of the computational domain.

channel height. The Schmidt number $Sc = \frac{\nu}{\Gamma}$, where Γ is the molecular diffusivity, is set to unity, leading to a Peclet number $Pe = \frac{u_\tau h}{\Gamma} = 150$. The dimensions of the domain, normalized by the half-channel height, are 5π along the streamwise (x) direction and π along the spanwise (z) direction. The flow configuration is shown in Fig. 1. The velocity and scalar equations are solved using a pseudo-spectral code. Fourier modes are adopted for the spatial discretization of the streamwise and spanwise directions, while Chebyshev polynomials are used in the wall-normal direction (y). The number of grid points is $197 \times 97 \times 96$ in the streamwise, wall-normal and spanwise directions respectively. In order to ensure adequate resolution, the grid is stretched along the wall-normal direction; The cells adjacent to the wall are placed at $\Delta y^+ \approx 0.08$, where superscript $(.)^+$ indicates quantities expressed in wall units. Along the streamwise and spanwise directions, uniform grid spacing is adopted.

The flow is maintained by a uniform pressure gradient imposed in the streamwise direction x. Regarding the velocity field, no-slip boundary conditions are applied at the top and bottom walls and periodic conditions are imposed in the other two directions. For the scalar field, zero-flux boundary conditions are imposed at the solid walls, whereas the scalar is removed in the proximity of the domain boundaries in the other two directions in order to restrict it from re-entering the domain from the opposite side.

RELEASE POINTS

We have performed a number of numerical experiments for each configuration, each time introducing the sensor at a different initial positions. The initial positions are isotropically distributed on a circle around the reference point for two-dimensional search and on a sphere for three-dimensional search, where the radius equals half the distance covered during a singel time step by the sensor when it is located inside the plume, denoted as d_o.

Mean values of various statistics relevant scalar source identification were evaluated by averaging over successful runs. For the two-dimensional search, 30 initial sensor positions are chosen for each reference point at planes located at different channel heights (Fig.2) where the scalar source is placed at $y^+ = 10, 30$ and 150 respectively. The streamwise and spanwise coordinates of the source location are $x = 1.15$ and $z = \pi/2$ respectively and are kept the same for all channel heights. The sensors are restricted to move in the corresponding x-z plane of the scalar source.

For the three-dimensional search, 32 initial sensor positions were chosen for a single reference point, whereas the sources location is placed at $y^+ = 150$. Details regarding

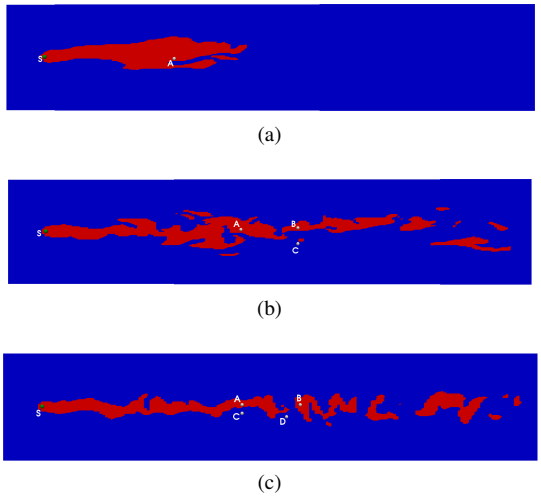

Figure 2: Release points of the sensors at planes extracted at (a) $y^+ = 10$, (b) $y^+ = 30$ and (c) $y^+ = 150$. Regions where concentration exceeds the threshold value are indicated by red color, where blue color is used to indicate regions with concentrations below the threshold value. Symbols S and A-D indicate the source and the release points respectively.

the spatial coordinates of the reference points at the corresponding x-z plane are shown in Table 1.

Table 1: Locations of reference points for sensor release (x, z) for all the cases

Configuration	A	B	C	D
Two-dimensional search				
$y^+ = 150$	(7,1.62)	(8.7,1.62)	(7,1.37)	(8.3,1.27)
$y^+ = 30$	(7,1.62)	(8.7,1.67)	(8.7,1.20)	-
$y^+ = 10$	(5,1.52)	-	-	-
Three-dimensional search				
$y^+ = 150$	(7,1.22)	-	-	-

SEARCH ALGORITHMS

Numerous searching algorithms can be found in literature in which the searcher adopts different behaviours, depending on its state. For simplicity, we have chosen surge-spiralling and casting algorithms, since they consider only two states; when inside the plume (sensing event) and when outside the plume (signal lost).

With respect to searching strategies, we have chosen surge-spiralling and casting algorithms, due to their simplicity and a small number of adjustable parameters in them. The casting algorithm (Fig. 3a) performs crossflow motions outside of the plume. If the sensor detects concentration above the threshold value, then it moves at an angle β with respect to the upflow direction when it is outside the plume. The sign of β is taken to be either positive or negative, depending on the relative angle between the sensor's heading

direction right after it enters the plume and the flow direction, so that the sensor moves towards the inner part of the plume, as indicated in Fig. 3a. This behavior is repeated until the sensor is out of the plume for a distance d_{lost}. Then, the sensor begins to cast, meaning that it starts traveling back and forth across the flow direction ($\pm\pi/2$ to upwind) in a progressively increasing amplitude until the plume is found, as suggested by Kennedy & Marsh (1974).

In the current study, the heading direction of the sensor is determined by the following expression:

$$\theta_s = \theta_f + \pi \pm \beta\,, \tag{1}$$

where θ_s denotes sensor's heading direction, θ_f corresponds to the flow direction, where β is chosen to be constant and equal to $\pi/3$, a choice also adopted by Russell *et al.* (2003). Eq. (1) is adopted once the sensor enters the plume and is kept unchanged until it exits. In order to account for the continuous increase of the crosswind scanning widths during the casting process, we have adopted the following iterative expression

$$d_c^{\eta+1} = d_c^{\eta} + n_r d_o\,, \tag{2}$$

where η denotes the current step after the sensor began to cast, and n_r denotes the progressive increase of the step size. For our computations, this value was set to 0.8 and it was kept fixed through all computations. Also, the sensor was considered off track after moving two consecutive steps outside of the plume, thus defining the distance d_{lost}.

We have also considered the surge-spiralling algorithm (Fig. 3b). This algorithm can adopt three different behaviors, depending on whether it is located inside or outside the plume. If the search starts from outside the plume, the sensor performs an outward Archimedean spiral motion with a spiral gap denoted by $d_{gap,1}$. If the sensor detects a concentration larger than the threshold, it surges upwind ($\beta = 0$ in eq. (1)) with a step size d_o chosen to equal the one adopted for the casting algorithm. Again, the heading direction θ_s is determined right after the sensor enters the plume, and it remains fixed until the sensor loses contact with the plume after it covers a distance d_{lost} outside the plume, in which case the sensor's behaviour switches to spiralling motion. This time, the sensor adopts a smaller gap $d_{gap,2}$ compared to the initial search gap $d_{gap,1}$, since the sensor has just exited the plume and it is assumed to be close to it, in contrast to the initial search starting outside the plume, in which case no prior information regarding plume's location can be used. The Archimedean motion is described by the following equation

$$r = a\theta\,, \quad a = d_{gap}/2\pi\,, \tag{3a}$$

$$\theta = \eta\,\pi/4\,, \tag{3b}$$

where r represents the radius of the spiral motion, a is a fixed constant and θ is the sensor turning angle.

We have also developed an extension of the surge-spiralling algorithm to account for three-dimensional searches. Briefly, the sensor surges upwind when it is inside the plume, while it performs helical motion outside of the plume, as shown in Fig. 6 in the results section. In order to construct a suitable expression for the helical motion,

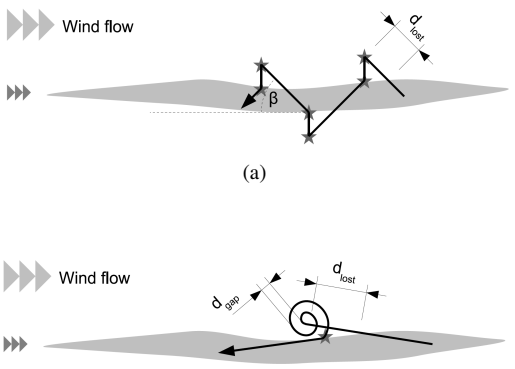

Figure 3: Sketch of (a) casting and (b) surge-spiraling (SS) algorithms, as provided by Lochmatter *et al.* (2008). The stars indicate where the wind direction is measured, whereas the grey region indicates the plume region.

we decompose the sensor motion into two parts, as shown in Fig. 4. The first considers the motion along a plane oriented perpendicular to the upwind direction, with local coordinates denoted as (x',y'), and z' is aligned to the upwind direction. The upwind direction was evaluated right after the sensor traveled distance d_{lost} outside the plume and is off target, and it remained fixed until the sensor re-entered the plume. Based on the local coordinate system, the sensor performs a spiralling motion as described by eq. (3), while the values for $d_{gap,1}$ and $d_{gap,2}$ are chosen to be equal to the corresponding values adopted for the two-dimensional cases. The second part considers the sensor motion along the upwind direction, denoted as z'. Many different expressions have been considered for the determination of z', however for the current study we have adopted

$$z' = \gamma\theta\,, \tag{4a}$$

where θ is the turning angle of the Archimedean motion, defined in Eq. (3b), and γ is a constant that determines how fast the sensor evolves along the upwind direction. After evaluation of the sensor location in the local frame, the corresponding global coordinates are obtained through the use of Euler angles. These angles are used to define the rotation matrix, denoted as R_{ij}, and the relation between the global and the local coordinates is given by

$$x_i' = x_i^o + R_{ij}x_j'\,, \tag{5}$$

where x_i^o is the location in global coordinates at which the sensor was deemed off track and started performing the helical motion.

We deem the search successful if the sensor manages to approach the source within a distance of 0.2 times the half-channel height h. In order to consider reference points sufficiently far away from the source, a large amount of DNS data was stored, corresponding to a time period $T^+ = 60$. If the sensor did not locate the source within this time horizon, the search was declared unsuccessful.

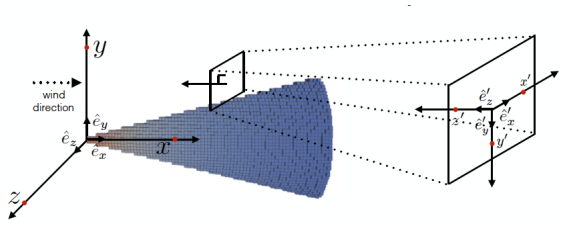

Figure 4: Sketch showing details of the decomposition process. The coloured region indicates the plume region.

One of the main objectives of the current study is to investigate the impact of the flow field on the search process. For example, if the sensor moves very rapidly, the flow is practically unchanged during the time horizon of the search, a limit at which the flow field can be assumed "frozen". On the other hand, if the sensor is moving very slowly it practically senses the presence of an averaged field. The third case is when the velocities of the sensor and the flow field are comparable. In this case, and for a sufficiently large number of steps, the evolution of the flow is expected to influence the performance of the algorithms. Based on the above arguments, an important parameter that can describe these effects is the velocity ratio, defined as

$$R_v = u_s/u_f\,, \tag{6}$$

where u_s is the sensor's averaged velocity during the search and u_f is a characteristic flow velocity. The reason for selecting the averaged and not the instantaneous sensor velocity, is because the sensor keeps a fixed speed while it is moving inside the plume, although its velocity can vary during the reacquisition process. We have chosen the reference points and the algorithms parameter carefully so that, for the intermediate state the relative velocities are comparable, in order to account for the effect of unsteadiness. Very large values of this parameter correspond to the limit of a "frozen" field as described above, whereas a value very close to zero suggests a very slow marching of the sensor. For the two-dimensional computations, the flow velocity is chosen to equal the mean streamwise velocity at the specific x-z plane, whereas the centerline mean velocity is adopted for the three-dimensional computations. Lastly, it is important to note that the frozen field corresponds to a snapshot of the turbulent flow field.

PERFORMANCE INDICES

During the evaluation process, a number of performance indices are computed. The first index is the success rate, defined as the ratio of the successful runs to the total number of runs, which measures the robustness of the corresponding algorithm. As already mentioned above, the run is considered to be successful if the moving sensor reaches the vicinity of the source within $T^+ = 60$. Additional important parameters are the distance ratios, defined as

$$R_{in} = L_{in}/L\,, \qquad R_{out} = L_{out}/L\,, \qquad R = \frac{L}{D}\,, \tag{7}$$

where L_{in} is the distance covered inside the plume, L_{out} is the distance covered outside the plume, L is the total distance and D is the displacement of the robot from the release point to the source. The minimum value of R is unity, a case at which the sensor surges straight upwind during the entire process.

RESULTS

All algorithms use binary odor information, that is they detect odor only if it exceeds a threshold value, while ignoring the gradation in concentration. In order to evaluate the performance of the algorithms, the computations used two different threshold values, 5% of the source intensity for the two-dimensional computations and 10% of the source intensity for the three-dimensional case.

Two dimensional search

Firstly we consider the two-dimensional motions. Due to the large number of reference points and performance indices, here we show selected results which illustrate the main trends of the analysis. We show results for searches at all three different channel heights. As discussed in detail by Cerizza *et al.* (2016), the wall-normal position significantly influences scalar dispersion and diffusion. Table 2 lists the performance indices for the case where the sensor is restricted to move on the x-z plane located at $y^+ = 150$ (channel centerline), starting from the reference point D. We have chosen this particular point, because it is positioned sufficiently far from the source so that the impact of the unsteadiness of the flow on the searching performance is appreciable. Also, this point is chosen so that the sensor starts its search outside of the plume, as shown in Fig 2c. We observe that the choice of R_v influences the performance of the algorithm. In particular, the casting algorithm provides higher success rate for finite velocity ratio compared to the frozen case, even though the sensor spends more time inside the plume for the frozen case compared to the unsteady one. Two main processes characterize the evolution of the field: diffusion and dispersion. At the channel centerline, dispersion provides an effective redistribution of the scalar field by the velocity to points such as D in Fig. 2c which is initially located away from the plume centerline. Better performance is achieved for $R_v = 0$. This outcome was expected, since at this limit the scalar field is assumed to be averaged, which means that the plume becomes continuous while it extends to large distances, as shown in Fig. 5.

Table 2: Estimation performance when a sensor starts inside a scalar plume at y^+ = 150

Algorithm \ Indices	Success Rate	R_{in}	R_{out}	R
Casting				
$R_v \to \infty$	8/30	0.381	0.619	4.425
$R_v = 8.90$	30/30	0.266	0.734	6.451
$R_v \to 0$	30/30	0.519	0.480	3.472
Surge-Spiralling				
$R_v \to \infty$	30/30	0.714	0.286	1.285
$R_v = 4.49$	30/30	0.477	0.523	1.927
$R_v \to 0$	30/30	0.831	0.169	1.08

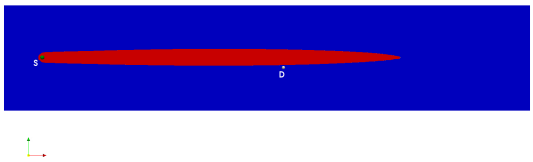

Figure 5: Mean scalar field along the x-z plane at $y^+ = 150$. Regions where concentration exceeds the threshold value are indicated by red color, where blue color is used to indicate regions with concentrations below the threshold value. Symbols S and D indicate the source and the release point respectively.

Table 3 shows details of the performance indices when the search is performed on a plane located outside the buffer layer, at $y^+ = 30$. Here we show results when the reference point is located at C based on the same arguments as for the centerline case. Again, we see a similar impact of the velocity ratio on the success rate as the previous case, while again best performance is achieved at the limit of the averaged field. Table 4 shows the corresponding comparison

Table 3: Estimation performance when a sensor starts outside a scalar plume at y^+ = 30

Algorithm \ Indices	Success Rate	R_{in}	R_{out}	R
Casting				
$R_v \to \infty$	30/30	0.341	0.686	5.263
$R_v = 12.05$	24/30	0.216	0.784	7.692
$R_v \to 0$	30/30	0.531	0.469	3.460
Surge-Spiralling				
$R_v \to \infty$	0/30	-	-	-
$R_v = 4.86$	30/30	0.499	0.501	1.776
$R_v \to 0$	30/30	0.863	0.137	1.134

for the plane located inside the buffer layer at $y^+ = 10$. We observe that the algorithm's performance is practically insensitive to the choice of velocity ratio, leading to similar values for the performance indices. This happens mainly because the diffusion effects become significant close to the wall, resulting to an excessive dissipation of the scalar field, which makes the scalar field more smoother, and closer to the time-averaged field.

Three dimensional search

Next, we have tested the performance of the proposed extension of the surge-spiralling algorithm for three dimensional motions. We consider the case where the source is placed at $y^+ = 150$, while the sensor release point is chosen to be initially outside of the plume. The scalar-detection threshold is 10% of the source intensity. Table 5 reveals the robustness of the proposed algorithm for all velocity ratios,

Table 4: Estimation performance when a sensor starts inside a scalar plume at y^+ = 10

Algorithm \ Indices	Success Rate	R_{in}	R_{out}	R
Casting				
$R_v \to \infty$	30/30	0.709	0.290	2.755
$R_v = 5.16$	30/30	0.668	0.332	2.890
$R_v \to 0$	30/30	0.687	0.313	2.786
Surge-Spiralling				
$R_v \to \infty$	30/30	1.0	0.0	1.009
$R_v = 4.15$	30/30	1.0	0.0	1.009
$R_v \to 0$	30/30	1.0	0.0	1.005

Table 5: Estimation performance for 3D search

Algorithm \ Indices	Success Rate	R_{in}	R_{out}	R
$R_v \to \infty$	32/32	0.392	0.608	2.119
$R_v = 4.08$	32/32	0.363	0.637	2.336
$R_v \to 0$	32/32	0.546	0.454	1.818

even though the sensor spends most of its time outside the plume. Again, best performance is observed for $R_v = 0$. In Fig.6 we show the path taken by the sensor using the three-dimensional extension of the surge-spiraling algorithm in order to locate the source.

CONCLUSIONS

In the present study, we tested existing olfactory algorithms using velocity and scalar fields obtained by DNS of a fully developed channel flow. Several performance indices were proposed and evaluated. In addition, the ratio between the sensor velocity and a characteristic mean velocity of the flow field is taken into account in order to investigate the influence of the unsteadiness of the flow field on the algorithm performance. For the two-dimensional computations, three planes were chosen, located at different channel heights. We have observed that the evolution of the flow field significantly influences the results for the cases where the planes of motion are located outside the buffer layer, which can be attributed to dispersion being dominant in these regions: Dispersion advects the scalar to regions where diffusion alone would not reach, thus increasing the probability for the sensor to detect a signal above the threshold value. For the case where the source is located inside the buffer region the diffusion effects become important, making the scalar field smoother so that the algorithm becomes insensitive to the value of the velocity ratio parameter. We have also proposed an extension of the surge-spiralling to three dimensional searches. The algorithm was shown to be robust regardless the choice of the velocity ratio. The present results suggest that the velocity ratio between sensor movement and characteristic flow velocity should be taken into account, and an employed algorithm should be chosen accordingly in designing scalar source estimation system. Although we observe different trends in three-dimensional

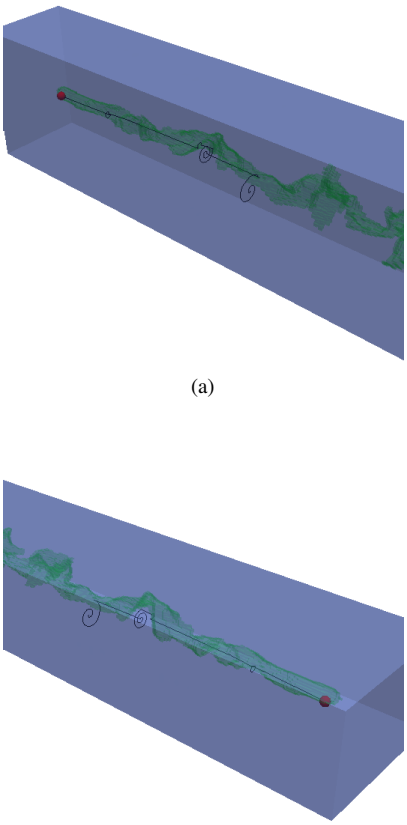

(a)

(b)

Figure 6: Trajectory of the sensor until it reached the source. Red sphere indicates the source, where green region indicates the plume. (a) and (b) show the same path, but from different viewpoints.

search from those in two-dimensional search, more detailed analysis is necessary to understand how the increase in the dimensionality influences the resultant searching performance.

REFERENCES

Cerizza, D., Sekiguchi, W., Tsukahara, T., Zaki, T. & Hasegawa, Y. 2016 Reconstruction of scalar source intensity based on sensor signal in turbulent channel flow. *Flow. Turbul. Combust.* **97**, 1211–1233.

Ishida, H., Wada, Y. & Matsukura, H. 2012 Chemical sensing in robotic applications: A review. *IEEE Sens. J.* **12**, 3163–3173.

Kennedy, S. & Marsh, D. 1974 Pheromone-regulated anemotaxis in flying moths. *Science 184.4140* **184**, 999–1001.

Lochmatter, T., Raemy, X., Matthey, L., Indra, S. & Martinoli, A. 2008 A comparison of casting and spiraling algorithms for odor source localization in laminar flow. In *Proceedings of the 2008 IEEE International Conference on Robotics and Automation (ICRA2008)*, pp. 1138–1143. Pasadena, CA, USA, May 19-23.

Muller, M. & Wehner, R. 1994 The hidden spiral: systematic search and path integration in desert ants, cataglyphis fortis. *J. Comp. Physiol. A* **175**, 525530.

Russell, R., Bab-Hadiashar, A., Shepherd, R. & Wallace, G. 2003 A comparison of reactive robot chemotaxis algorithms. *Robot. Auton. Syst.* **45**, 83–97.

Voges, N., Chaffiol, A., Lucas, P. & Martinez, D. 2014 Reactive searching and infotaxis in odor source localization. *PLoS Comput. Biol.* **10(10)**, e1003861.